Journal of Applied Polymer Science

# Preparation and Photocurrent Generation of an Electrostatically Self-Assembled Film of Hemicyanine and Poly(4-styrenesulfonic acid-*co*-maleic acid)

**Xiaoyan Lin,[1] Lihua Gao,[1] Xi Chen,[2] Jianmin Qi,[1] Kezhi Wang[2]**

[1]Department of Chemistry, School of Science, Beijing Technology and Business University, Beijing 100048, China

[2]College of Chemistry, Beijing Normal University, Beijing 100875, China

Correspondence to: L. H. Gao (E-mail: gaolh@th.btbu.edu.cn)

**ABSTRACT:** In this article, we report on electrostatically self-assembled thin films prepared by the alternative immersion of quartz-coated and indium tin oxide coated glass substrates in aqueous solutions of a copolymer of poly(4-styrenesulfonic acid-*co*-maleic acid) (PSSMA) and a hemicyanine of (*E*)−1,1′-(propane-1,3-diyl)bis{4-[4-(dimethylamino)styryl]pyridinium} bromide ($H^3Br_2$). The films were studied by means of ultraviolet–visible absorption and X-ray photoelectron spectroscopies, scanning electron microscopy, and photoelectrochemical measurements. When irradiated with white light, the PSSMA/$H^3$ monolayer film gave a stable cathodic photocurrent. The effects of the applied bias voltages, layer numbers of the $(PSSMA/H^3)_n$ films (where *n* stands for the number of bilayer films on both sides of the substrates), light intensities, pH value, and electron acceptor on the photocurrent generation of the $(PSSMA/H^3)_n$ film were examined. © 2013 Wiley Periodicals, Inc. J. Appl. Polym. Sci. **2014**, *131*, 39871.

**KEYWORDS:** films; optical and photovoltaic applications; optical properties

Received 16 May 2013; accepted 19 August 2013

**DOI: 10.1002/app.39871**

## INTRODUCTION

Since Decher[1] first reported an easy, inexpensive, and effective technique for the construction of multilayer polymer films of oppositely charged polyelectrolytes, this layer-by-layer self-assembly technique has been extensively adopted to construct layered polymer thin-film materials with fine control over thickness, composition, and chemical functionalities.[2–4] Hemicyanine derivatives, with a donor–π-acceptor structure, are a class of important organic molecules, which have been extensively investigated because of their multifunctionality, including nonlinear optical functionality,[5–8] photoelectric conversion,[8–16] and fluorescence properties.[17–20] Huang and coworkers[8–16] studied the photoelectric conversion properties of Langmuir–Blodgett (LB) films of amphiphilic hemicyanine dyes, but the LB technique is constrained by delicate equipment and substrate sizes and shapes. Not only can the electrostatic self-assembly technique overcome the aforementioned shortcomings but it can also assemble two or more kinds of functional materials in a controllable way. Our group has long been interested in electrostatically self-assembled films made of hemicyanines and polyoxometalates (POMs) and their photoelectrochemical and second-order nonlinear optical properties.[21–33] Organic polymers have excellent chemical and mechanical stabilities and good film-forming properties compared with POMs. To our knowledge, electrostatically self-assembled films of polymers and hemicyanine have not been reported so far. In this article, we report a new electrostatically self-assembled film made of a copolymer containing both weakly and strongly acidic pendant groups, poly(4-styrenesulfonic acid-*co*-maleic acid) (PSSMA; see Figure 1 for molecular structure) and a hemicyanine dimer of (*E*)−1,1′-(propane-1,3-diyl)bis{4-[4-(dimethylamino)styryl]pyridinium} bromide ($H^3Br_2$; see Figure 1 for molecular structure). The photoelectrochemical properties of the $(PSSMA/H^3)_n$ film (where *n* stands for the number of bilayer films on both sides of the substrates) modified indium tin oxide (ITO) electrode and the effects of the applied bias voltage, layer number of film, light intensity (*x*), pH value, and addition of the electron acceptor in the electrolyte solution on photocurrent generation are reported as well.

## EXPERIMENTAL

### Materials

Sodium salt of the copolymer of 4-styrenesulfonic acid (SS) and maleic acid (MA) at SS:MA molar ratio of 3:1 (abbreviated as

Additional Supporting Information may be found in the online version of this article.

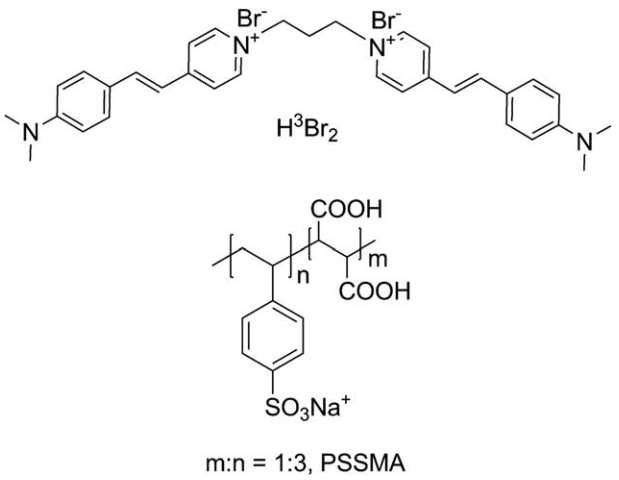


**Figure 1.** Structures of $H^3Br_2$ and PSSMA.

PSSMA) with a molecular weight of 20,000 g/mol and (3-aminopropyl)trimethoxysilane (99%) were purchased from Acros and Aldrich, respectively, and were used without further purification. $H^3Br_2$ was synthesized according to the route shown in Figure 2, and the synthetic details are described later.

A solution of 4-methylpyridine (3.92 mL, 40 mmol) and 1,3-dibromopropane (2.04 mL, 20 mmol) in 50 mL of absolute ethanol (EtOH) was refluxed under $N_2$ for 24 h. When the reaction mixture was cooled to ambient temperature, a pink precipitate of 1,1-(propane-1,3-diyl)bis(4-methylpyridinium) bromide formed and was filtered and recrystallized from EtOH–ethyl ether. A solution of 1,1-(propane-1,3-diyl)bis(4-methylpyridinium) bromide (1.16 g, 3 mmol) and 4-(dimethylamino)benzaldehyde (0.90 g, 6 mmol) in absolute EtOH (25 mL) and piperidine (1 mL) was refluxed for 7 h and cooled to ambient temperature. A reddish brown precipitate formed and was filtered and recrystallized from EtOH to give 1.02 g of $H^3Br_2$ in a 52.3% yield.

mp = 272–275°C. Anal. Calcd for $C_{33}H_{38}N_4Br_2$: C, 60.93%; H, 5.89%; N, 8.61%. Found: C, 61.40%; H, 5.81%; N, 8.71%. IR (KBr): 2920 (w), 1642 (w), 1585 (vs), 1526 (s), 1474 (w), 1435 (w), 1362 (m), 1332 (m), 1044 (w), 969 (w), 944 (w), 819 (w). $^1$H-NMR (500 MHz, DMSO-$d_6$, $\delta$, ppm): 8.79–8.81 (4H, d, —$C_5H_4N$), 8.09–8.11 (4H, d, —$C_5H_4N$), 7.95–7.98 (2H, d, —CH═), 7.59–7.61 (4H, d, —Ar—H), 7.19–7.22 (2H, d, —C═C—H), 6.78–6.80 (4H, d, —Ar—H), 4.55–4.58 (4H, t, N—$CH_2$), 3.04 [12H, s, —$N(CH_3)_2$], 2.51–2.62 (2H,s, $NCH_2$—$CH_2$).

### Film Preparations

Quartz substrates were used for ultraviolet–visible (UV–vis) absorption measurements. ITO-coated glass substrates were used for photoelectrochemical experiments. The protonation and silanization of these substrates were done as described before.[21] The obtained substrates were then immersed in a PSSMA aqueous solution (2 mg/mL) for 60 min to adsorb the negatively charged PSSMA monolayer. After they were washed with water and dried with air, the resulting PSSMA-coated substrate was placed for 60 min in a $1.0 \times 10^{-3}$ $M$ $H^3Br_2$ aqueous solution (see the optimal time curves for the deposition of PSSMA and $H^3Br_2$ shown in Figure S1 in the Supporting Information), washed with water, and dried with air. Repetition of the previous two steps yielded the $(PSSMA/H^3)_n$ multilayer film, as shown schematically in Figure 3. $Br^-$, the counter ion of the film-forming component of $H^3$, remained in the solution, as revealed by X-ray photoelectron spectroscopy (XPS; see discussions in the following XPS section).

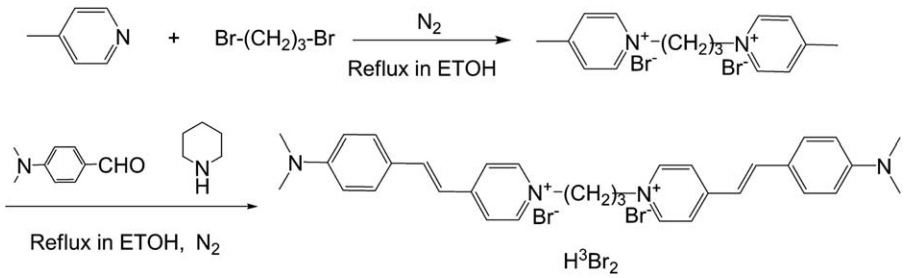


**Figure 2.** Synthetic route to $H^3Br_2$.

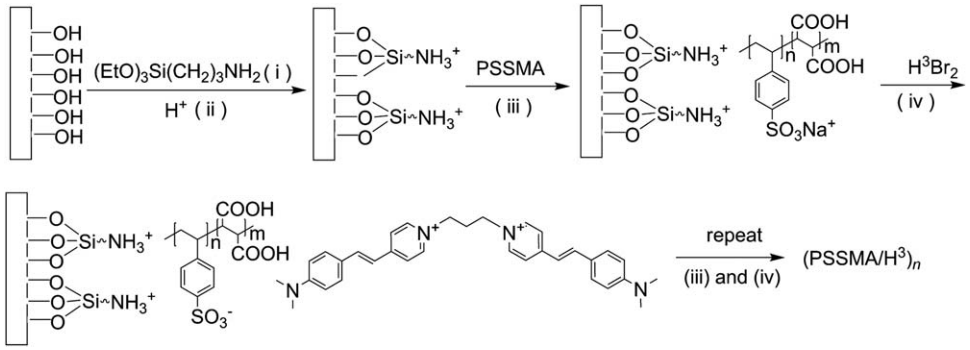


**Figure 3.** Schematic illustration of the assembly process of the multilayer film $(PSSMA/H^3)_n$.

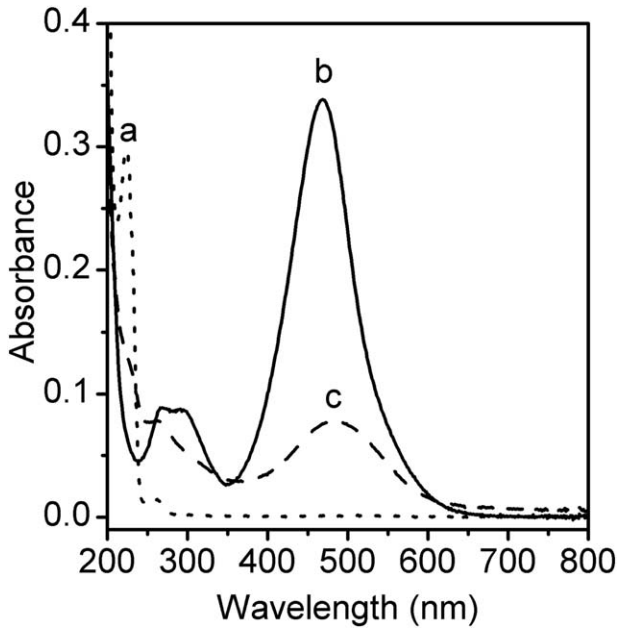


**Figure 4.** UV–vis absorption spectra of the (a) PSSMA in $H_2O$, (b) $H^3Br_2$ in $H_2O$, and (c) multilayer $(PSSMA/H^3)_6$ film.

### Physical Measurements

UV–vis spectra were measured on a GBC Cintra 10e UV–vis spectrophotometer. The surface morphologies of the deposited films were studied with scanning electron microscopy (SEM; Hitachi S-4800-II). XPS spectra were measured on an Axis Ultra X-ray photoelectron spectrometer from Thermo Fisher with Al Kα irradiation on an ESCA-250 system. For calibration, the C1s line was set at 286.4 eV as a standard. Photoelectrochemical measurements were conducted on an assembly of a xenon lamp (500-W) light source and a CHI-660D electrochemical analyzer. All of the electrochemical and photoelectrochemical experiments were performed in a specially designed three-electrode conventional cell at the ambient laboratory temperature in a 0.1*M* $Na_2SO_4$ aqueous solution. The working electrodes were ITO substrates modified with the $(PSSMA/H^3)_n$ films for photoelectrochemical measurements. A platinum wire and a saturated calomel electrode (SCE) were used as the counter electrode and reference electrode, respectively. For the photoelectrochemical experiments, white-light irradiation on the film-modified ITO electrode (effective area = 0.28 $cm^2$) was given by a xenon lamp (500 W) through an IR cutoff filters (730 nm > Wavelength > 325 nm). A monochromatic light for the measurement of the photocurrent action spectrum was obtained from a xenon lamp fitted with optical interference filters. The value of *x* was measured with a model ST-900M photometer.

## RESULTS AND DISCUSSION

### UV–Vis Absorption Spectra

The UV–vis absorption spectra for the PSSMA and $H^3Br_2$ in aqueous solutions and the multilayer film of $(PSSMA/H^3)_6$ are compared in Figure 4 (see also Table I). The PSSMA aqueous solution exhibited a strong $\pi \rightarrow \pi^*$ absorption band at 226 nm due to the sulfonated phenyl moiety[34] and a weak $n \rightarrow \pi^*$ absorption band at 261 nm. The $H^3Br_2$ aqueous solution showed a $\pi \rightarrow \pi^*$ absorption band at 269 nm and a relatively strong intramolecular charge transfer (ICT) absorption band at 469 nm.[30] The multilayer film of $(PSSMA/H^3)_6$ exhibited two absorption bands at 261 and 486 nm; the former was obviously stronger than the latter; this was opposite to the spectral feature of the $H^3Br_2$ aqueous solution and indicated that the former band was the superposition of the PSSMA-based $n \rightarrow \pi^*$ absorption and the $H^3$-based $\pi \rightarrow \pi^*$ absorption and that the band at 486 nm in the film was contributed by the $H^3$-based ICT absorption because of the fact that PSSMA did not absorb in the visible region. The previous results indicate that the two film-forming components of PSSMA and $H^3$ were successfully assembled into the film. By comparison of the ICT absorption band position of $H^3Br_2$ in aqueous solution with that in the $(PSSMA/H^3)_n$ film, a redshift of 17 nm was observed for the $(PSSMA/H^3)_n$ film with respect to the $H^3Br_2$ aqueous solution. Such a redshifted behavior was already observed in our previously reported electrostatically self-assembled films made of hemicyanines and POMs[21–33] and was ascribed to the formation of J-aggregates of the hemicyanine in the film and/or the occurrence of the charge transfer between PSSMA and $H^3$.[35] In contrast, blueshifts of 13, 30, and 36 nm were previously reported for monolayer LB films of similar hemicyanines of (*E*)-*N*-octadecyl-4-[2-(4-dimethylamino)phenyl]ethenyl pyridinium iodide (OMPI), (*E*)-*N*-hexadecyl-4-[2-(4-diethylamino)phenyl]ethenyl pyridinium iodide, and (*E*)-*N*-octadecyl-4-[2-(4-diethylamino)-phenyl]ethenyl pyridinium iodide (OEPI), respectively.[12,36]

Figure 5 shows the UV–vis absorption spectra of the increased layer numbers of the films on a quartz substrate. Clearly, the absorbances at 261 and 486 nm increased linearly with *n* in the $(PSSMA/H^3)_n$ films (see the inset in Figure 5) with correlation coefficients of 0.99462 and 0.99305, respectively; this demonstrated that equal amounts of PSSMA and $H^3$ were transferred into the film at each deposition cycle. The surface concentration of $H^3$ in the film ($\Gamma$) was calculated to be $3.50 \times 10^{-10}$

**Table I.** UV–Vis Absorption Spectral Data

| Compound or film | $\lambda_{max}$ (nm) | $\Delta\lambda_{max}$ (nm) | $A_{vis}$ | $\Gamma$ (mol/$cm^2$) | Reference |
|---|---|---|---|---|---|
| PSSMA aqueous solution | 224, 264 | | | | This work |
| $H^3$ aqueous solution | 269, 469 | | | | This work |
| $(PSSMA/H^3)_n$ film | 261, 486 | 17 | $2.06 \times 10^{-2}$ | $3.50 \times 10^{-10}$ | This work |
| $(SiW_{12}/H^3)_n$ film | 271, 504 | 35 | $3.80 \times 10^{-2}$ | $4.62 \times 10^{-10}$ | 30 |

$\lambda_{max}$, maximum absorption wavelength; $\Delta\lambda_{max}$, the difference between the absorbance of films and that of the corresponding hemicyanine solution in the visible region (nm); $A_{vis}$, absorbance of the monolayer film in the visible region.

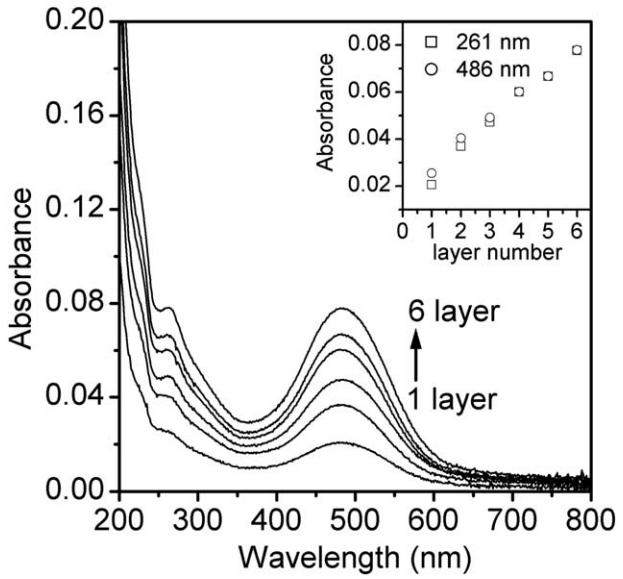


**Figure 5.** UV–vis absorption spectra of the $(PSSMA/H^3)_n$ multilayers with varied numbers of layers ($n = 1$–6) on both sides of quartz. The inset is a plot of the absorbances of the films at 261 and 486 nm versus the layer number.

mol/cm$^2$ on the basis of eq. (1), which was derived from the Lambert–Beer law modified for two-dimensional concentration:[37]

$$\Gamma = 10^{-3} D/\varepsilon \quad (1)$$

where $D$ is the absorbance per layer for the $H^3$ molecule in the film at 486 nm, which was derived to be 0.0055 from the slope in the linear relationship in the inset of Figure 5, and $\varepsilon$ is the molar extinction coefficient for the $H^3$ molecule in the film at 486 nm, which was supposed to be approximately equal to $\varepsilon_{469nm} = 1.58 \times 10^4\ M^{-1}\ cm^{-1}$ for $H^3Br_2$ in aqueous solution.

### XPS

The full-range and high-resolution XPS spectra of the $H^3Br_2$ powder and $(PSSMA/H^3)_4PSSMA$ thin film are shown in Figures 6 and S2 (in the Supporting Information), respectively. As clearly shown in Figure 6, the Br3d XPS peak of bromide ions in the $H^3Br_2$ powder (68.7 eV) disappeared in the spectrum of the thin film; this indicated that the bromide ions still left in the solution as cationic $H^3$ and PSSMA polyanions were transferred by electrostatic attraction from their aqueous solutions into the film. The appearance of the double N1s peaks at 401.1 and 402.9 eV for the $H^3Br_2$ powder (see high-resolution XPS spectra in Figure S2) indicated the presence of two kinds of nitrogen atoms in the $H^3Br_2$ powder, which were related to the dimethylamino and pyridinium nitrogen atoms and shifted to the higher and lower binding energies of 401.8 and 402.6 eV for the film, respectively; these shifts in the N1s binding energies were attributed to the occurrence of charge transfer between $H^3$ and PSSMA in the film. Moreover, the S2p XPS peak, which originated from the film-forming component of PSSMA, appeared expectedly in the XPS spectrum of the film.

### SEM

Because the film surface morphology could be central to the photoelectric conversion performance,[38] we studied the surface

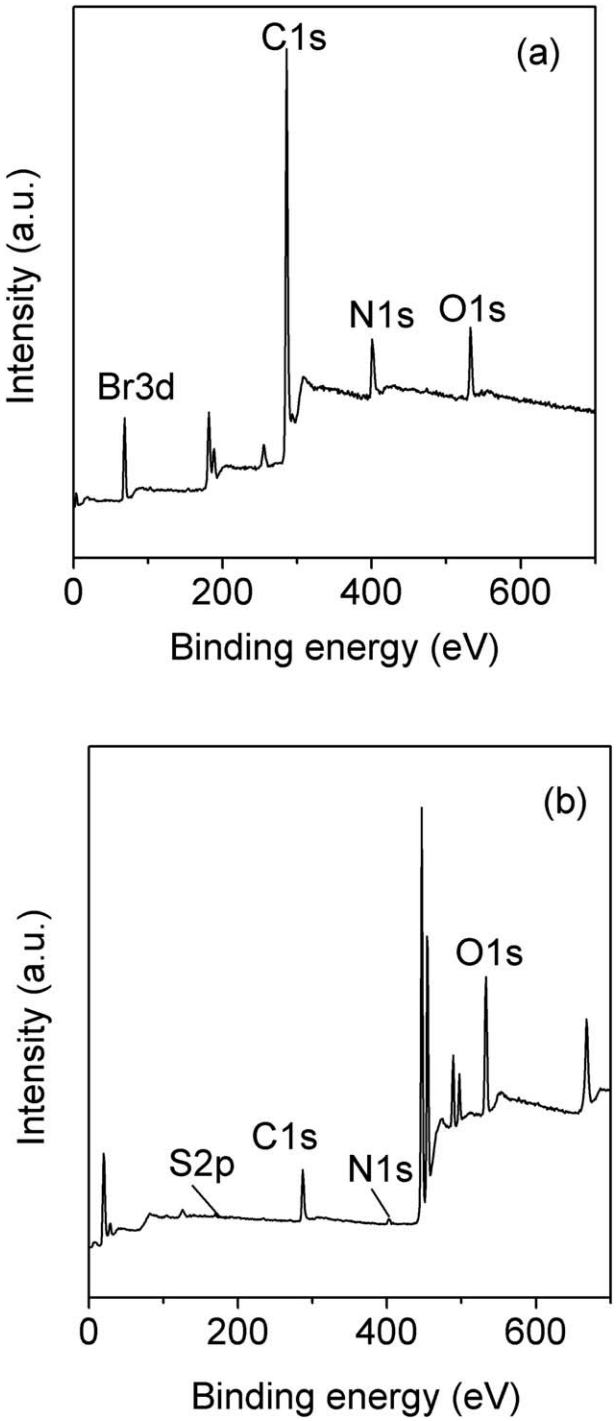


**Figure 6.** Full-range XPS spectra of the (a) $H^3Br_2$ powder and (b) $(PSSMA/H^3)_4PSSMA$ thin film.

morphologies of the bare ITO, ITO/$(PSSMA/H^3)_4$, and ITO/$(PSSMA/H^3)_4PSSMA$ films (see Figure S3). The surface of the bare ITO seemed to be relatively rough and formed by variable shapes and sizes of islands with platelike structures (Figure S3a), whereas the surface of the multilayer film of ITO/$(PSSMA/H^3)_4$, with $H^3$ being the outmost layer, seemed to be smooth and composed of small nanosized grains (Figure S3b in the Supporting Information). When one more layer of PSSMA

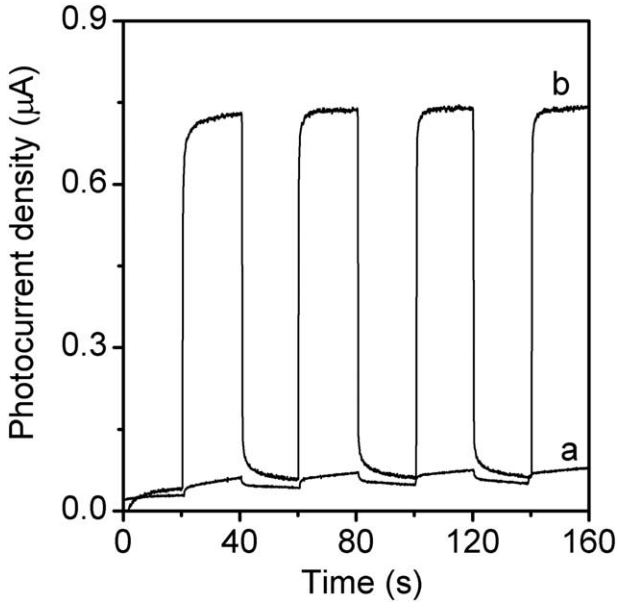


**Figure 7.** Photoelectric responses of the (a) ITO/PSSMA and (b) ITO/PSSMA/$H^3$ film electrodes in the 0.1*M* $Na_2SO_4$ electrolyte solution with 100 mW/cm$^2$ white-light irradiation at zero-bias voltage versus SCE.

was covered onto the ITO/$(PSSMA/H^3)_4$ film to form the ITO/$(PSSMA/H^3)_4$PSSMA film, the grains became smaller and more closely packed (Figure S3c in the Supporting Information).

### Photocurrent Generation Behavior from the $(PSSMA/H^3)_n$ Film Modified ITO Electrode

The photocurrent–time plots of the ITO/PSSMA and ITO/PSSMA/$H^3$ film electrodes in a 0.1*M* $Na_2SO_4$ electrolyte solution with a pH of 4.0 are compared in Figure 7. As shown in Figure 7, the monolayer $(PSSMA/H^3)_1$ film modified ITO electrode exhibited a stable cathodic photocurrent density (*I*) of 2.39 $\mu$A/cm$^2$ when illuminated with white light (100 mW/cm$^2$, $730 > \lambda > 325$ nm) at zero-bias voltage versus SCE; this was prompt and reproducible under several on/off cycles of irradiation. In contrast, the ITO electrode covered with only monolayer PSSMA without $H^3$ showed negligibly small cathodic photocurrents under the same experimental conditions; this indicated that the cathodic photocurrents originated from the hemicyanine $H^3$.

In comparison with the photocurrents generated by hemicyanine derivative film-modified electrodes (Table II), we observed that the *I* value of 2.39 $\mu$A/cm$^2$ for the $(PSSMA/H^3)_1$ film was about 6.2- and 4.3-fold greater than 0.33 and 0.45 $\mu$A/cm$^2$ for LB films of OMPI and OEPI, respectively. The enhanced *I* values observed for the $(PSSMA/H^3)_1$ film with respect to those for the LB films were ascribed to the formation of *J* aggregates of the $H^3$ molecules in the $(PSSMA/H^3)_1$ film, which was favorable for photoelectric conversion, whereas OMPI and OEPI in the monolayer LB films that exhibit hypsochromically shifted absorption band, are called the *H*-aggregates, which was unfavorable for photoelectric conversion.[12] The previous results demonstrate that the introduction of PSSMA into the hemicyanine-modified electrode was an effective approach for enhancing the photocurrent through the control of the formation of *J* aggregates. Moreover, the *I* value (2.39 $\mu$A/cm$^2$) for the $(PSSMA/H^3)_1$ film was 5.8-fold greater than the 0.35 $\mu$A/cm$^2$ previously reported for the electrostatically self-assembled $(H_4SiW_{12}O_{40}/H^3)_1$ film.[30]

**Table II.** Photocurrents Generated from the Hemicyanine-Film-Modified Electrodes

| Film | *I* ($\mu$A/cm$^2$) | References |
|---|---|---|
| $(PSSMA/H^3)_1$[a] | 2.39 | This study |
| $(SiW_{12}/H^3)_1$[a] | 0.35 | 30 |
| OMPI LB film[b] | 0.33 | 12 |
| OEPI LB film[b] | 0.45 | 12 |

[a] Irradiated by 100 mW/cm$^2$ white light.
[b] Irradiated by 86 mW/cm$^2$ white light.

### Effects of the Bias Voltages on the Photocurrent Generation of the $(PSSMA/H^3)_n$ Film

A plot of the observed *I* values versus the bias voltage for the monolayer $(PSSMA/H^3)_1$ film on the ITO electrode immersed in a 0.1*M* $Na_2SO_4$ aqueous solution with a pH of 4.0 is shown in Figure 8. We observed that the more negative the bias voltages were, the larger the photocurrents were; this indicated that the photocurrents generated from the $(PSSMA/H^3)_1$ film were cathodic; that is, the electrons flowed from the ITO electrode through the $(PSSMA/H^3)_1$ film into the electrolyte solution. The photocurrents showed a nonlinear dependence on the applied bias voltages in the range of $-0.3$ to 0.3 V versus SCE, but a good linear dependence on the applied bias voltages from $-0.3$ to $+0.1$ V versus SCE with the linear equation $I = 2.37 - 4.0V$ (V) with a correlation coefficient of $-0.99968$.

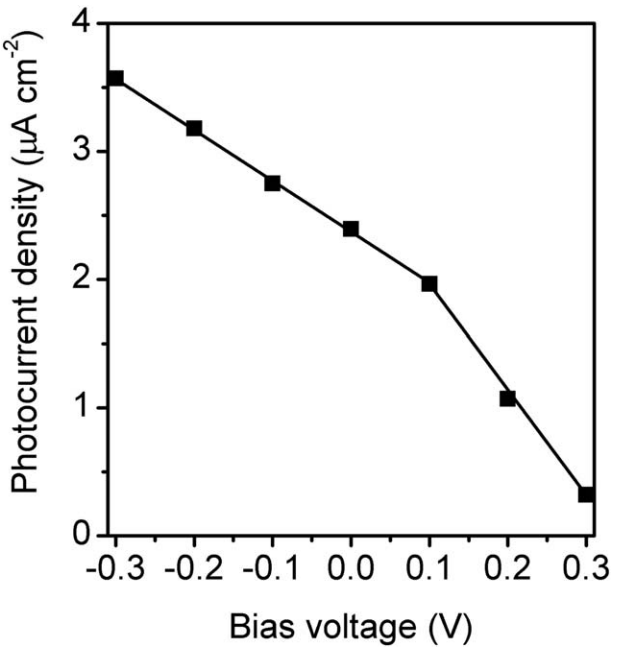


**Figure 8.** Effects of the bias voltage on the *I* values of the $(PSSMA/H^3)_1$ film on the ITO electrode in the 0.1*M* $Na_2SO_4$ electrolyte solution (pH 4.0) with 100 mW/cm$^2$ white-light irradiation.

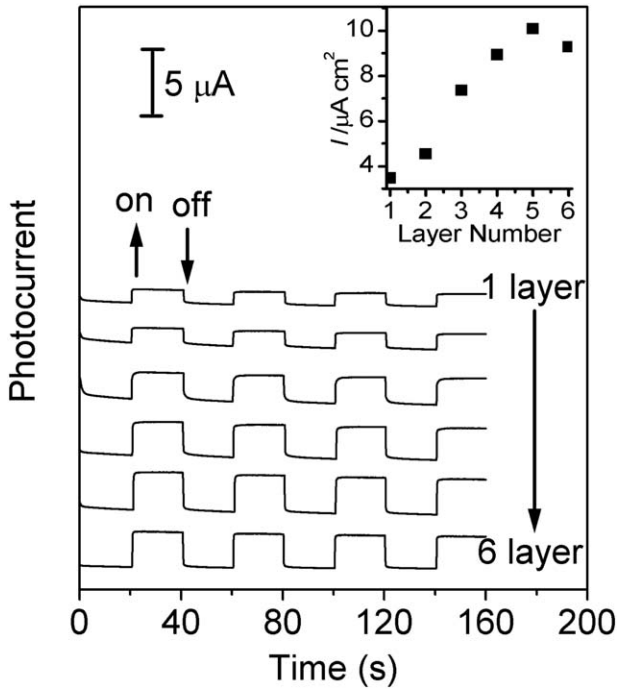


**Figure 9.** Photoelectric response of the $(PSSMA/H^3)_n$ film electrode with various layer numbers ($n = 1$–6) in an 0.1*M* $Na_2SO_4$ electrolyte solution with 100 mW/cm$^2$ white-light irradiation at −0.3 V versus SCE. The inset shows the dependence of the photocurrents at −0.3 V versus SCE on the number of deposited layers.

### Effect of the Film Layer Number on the Photocurrent Generation of the $(PSSMA/H^3)_n$ Film

The dependence of the photocurrents at −0.3 V versus SCE on the number of deposited layers of the $(PSSMA/H^3)_n$ ($n = 1$, 2, 3, 4, 5, and 6) films is shown in Figure 9. The cathodic *I* value increased with increasing layer number up to five layers (from 3.5 μA/cm$^2$ for a one-layer film to 10.1 μA/cm$^2$ for a five-layer film) and then decayed slightly with further increasing layer number. This was due to the fact that the increases in the layer number resulted in an increase in the electron-transport resistance, which offset the increased photon absorption and decreased the photocurrent generation accordingly.[39] At zero-bias voltage, a similar dependence of cathodic *I* on the layer number of the $(PSSMA/H^3)_n$ ($n = 1$, 2, 3, 4, 5, and 6) films was observed.

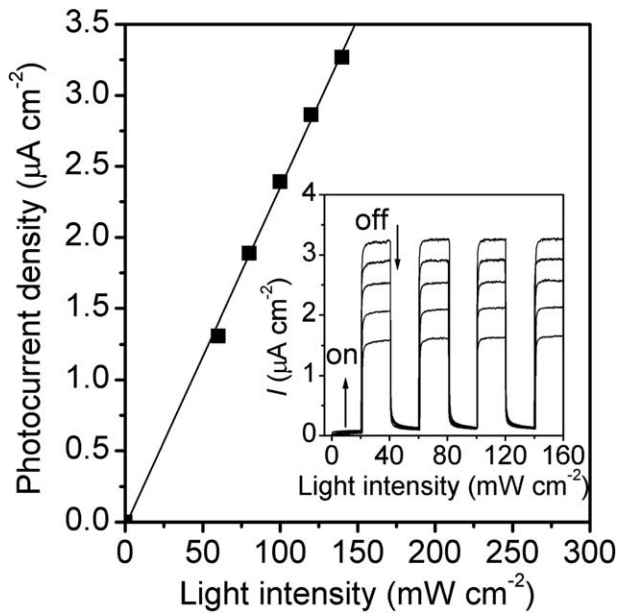


**Figure 10.** Relationship between the *I* values generated by the $(PSSMA/H^3)_1$ film electrode in a 0.1*M* $Na_2SO_4$ electrolyte solution at zero-bias voltage versus SCE and *x* values.

### Effect of *x* on the Photocurrent Generation of the $(PSSMA/H^3)_n$ Film

The dependence of the *I* value generated by the $(PSSMA/H^3)_1$ film electrode in the 0.1*M* $Na_2SO_4$ electrolyte solution at zero-bias voltage versus SCE on the incident *x* values is shown in Figure 10. *I* was found to increase linearly with *x* (mW/cm$^2$) up to 120 mW/cm$^2$, as described by the equation $I = 0.02378x$. This linear relationship was characteristic of unimolecular recombination.[40]

### Effect of the pH on the Photocurrent Generation of the $(PSSMA/H^3)_n$ Film

Figure 11 shows the effects of the electrolyte solution pH on the photocurrent intensities generated by the $(PSSMA/H^3)_1$ film electrode at zero-bias voltage versus SCE. The photocurrent intensities were found to increase with decreasing the pH values. It was reported that hemicyanine dyes underwent a facile trans→cis photoisomerization process upon irradiation,[41] which could take place more easily in an acidic environment;[8] this resulted in increases in the observed photocurrent intensities. Moreover, the proton dissociation of the weekly acidic

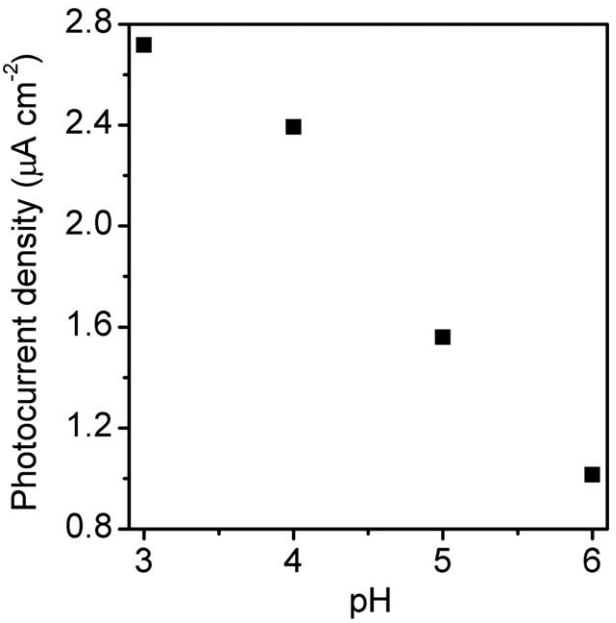


**Figure 11.** Effect of different pH values of the 0.1*M* $Na_2SO_4$ electrolyte solution on the *I* values generated from the monolayer $(PSSMA/H^3)_1$ film electrode with 100 mW/cm$^2$ white-light irradiation at zero-bias voltage versus SCE.

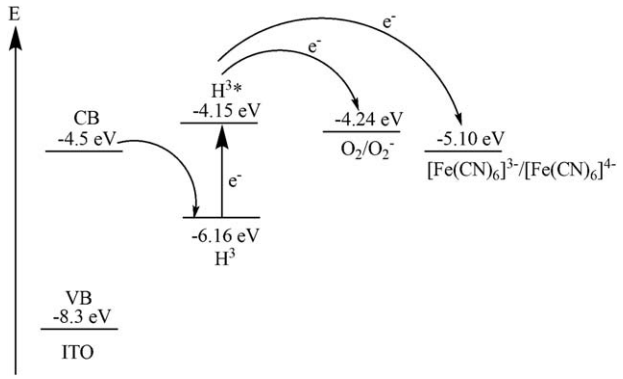


**Figure 12.** Schematic illustration of the electron-transfer mechanism.

carboxylic acid moieties in PSSMA was pH dependent and may have affected the photoisomerization of $H^3$ in the film.

### Effect of the Electron Acceptor on the Photocurrent Generation of the $(PSSMA/H^3)_n$ Film

The water-soluble electron acceptor of $[Fe(CN)_6]^{3-}$ was added to the 0.1*M* $Na_2SO_4$ electrolyte solution to further investigate the photocurrent polarity of the $(PSSMA/H^3)_2$ film. The result shows that the photocurrent increased by 24% at a $K_3[Fe(CN)_6]$ concentration of 10 $\mu M$; this demonstrated further that the film generated cathodic photocurrents, and this was consistent with the previously observed fact that the addition of an electron acceptor could promote the cathodic photocurrent generation.[10–12,28–32]

### Mechanism for Photocurrent Generation

The vacuum energy levels of the bottom of the conduction band (CB) and the top of the valence band (VB) of the ITO electrode were taken to be about −4.5 and −8.3 eV,[42,43] respectively. On the basis of an onset absorption wavelength ($\lambda_{onset}$) of 617 nm for $H^3$, a 0–0 transition energy was derived to be 2.01 eV according to eq. (2). On the basis of an experimentally observed onset reduction potential [$E_{onset(red)}$] of −0.59 V versus SCE for $H^3$ in the $(PSSMA/H^3)_n$ film and an energy of −4.74 eV for SCE with respect to the zero vacuum level,[44] the energies of the lowest unoccupied molecular orbital (LUMO) and the highest occupied molecular orbital (HOMO) of $H^3$ were calculated to be −4.15 and −6.16 eV, respectively, according to eqs. (2) and (3). The reduction potentials of $O_2$ and $[Fe(CN)_6]^{3-}$ were around −0.50 V[45] and 0.36 V versus SCE; these were converted to vacuum energy levels of −4.24 and −5.10 eV, respectively. With these values, the energy level diagram of the photoelectrochemical cell studied here was constructed and is shown in Figure 12. Upon the photoexcitation of the sensitizer $H^3$, the electron was promoted from the HOMO to the LUMO to form an electron-hole pair, the exciton. An electron flow could occur thermodynamically and favorably from the conductive band of the ITO electrode to the HOMO of $H^3$ and from the LUMO of $H^3$ into the electrolyte (a process of the exciton separation), where the electron was accepted by $O_2$ or $[Fe(CN)_6]^{3-}$. Namely, a net electron flow took place from the ITO electrode through the sensitizer $H^3$ and into the electrolyte; this produced the cathodic photocurrent. Such an exciton separation and charge-transport process was in contrast with that reported in conventional dye-sensitized solar cells,[45–49] where an anodic photocurrent was usually observed:

$$\Delta E^{00} = E_{LUMO} - E_{HOMO} = 1240/\lambda_{onset} \quad (2)$$

$$E_{LUMO}\,(eV) = \left[-4.74 - E_{onset\,(red)}\right] \quad (3)$$

## CONCLUSIONS

An electrostatically self-assembled film was prepared by the alternating adsorption of a polyanion of PSSMA and a cationic hemicyanine dimer of $H^3$. The UV–vis absorption spectra showed that the equal amounts of the two film-forming components were transferred into the films after each deposition cycle and that the charge transfer between these two film-forming components could occur and *J* aggregates could be formed in the films. The $(PSSMA/H^3)_n$ composite film modified electrodes exhibited enhanced stable photocurrents with respect to the previously reported $(H_4SiW_{12}O_{40}/H^3)_1$ film and LB films of similar hemicyanine dye modified electrodes. The polarity of the photocurrent was evidenced to be cathodic by examination of the dependence of the photocurrents on bias voltages, and the addition of the electron acceptor to the electrolyte solution.

## ACKNOWLEDGMENTS

Financial support by the National Natural Science Foundation of China (contract grant numbers 21371018, 21171022, 20971016, and 90922004), Beijing Natural Science Foundation (contract grant number 2092011), Scientific Research Foundation of Graduate School of Beijing Technology and Business University, and Analytical and Measurements Fund of Beijing Normal University.

## REFERENCES

1. Decher, G. *Science* **1997**, *277*, 1232.
2. Son, J. Y.; Kim, C. H.; Cho, J. H.; Shin, Y. S.; Shin, Y. H.; Jang, H. M. *J. Electrochem. Soc.* **2011**, *158*, D546.
3. Kharlampieva, E.; Kozlovskaya, V.; Sukhishvili, S. A. *Adv. Mater.* **2009**, *21*, 3053.
4. Volodkin, D.; Skirtach, A.; Möhwald, H. *Polym. Int.* **2012**, *61*, 673.
5. Ashwell, G. J.; Hargreaves, R. C.; Baldwin, C. E.; Bahra, G. S.; Brown, C. R. *Nature (London)* **1992**, *357*, 393.
6. Wang, K. Z.; Huang, C. H.; Xu, G. X.; Xu, Y.; Liu, Y. Q.; Zhu, D. B.; Zhao, X. S.; Xie, X. M.; Wu, N. Z. *Chem. Mater.* **1994**, 6, 1986.
7. Huang, C. H.; Wang, K. Z.; Xu, G. X.; Zhao, X. S.; Xie, X. M.; Xu, Y.; Liu, Y. Q.; Xu, L. G.; Li, T. K. *J. Phys. Chem.* **1995**, *99*, 14397.
8. Xia, W. S.; Huang, C. H.; Zhou, D. *J. Langmuir* **1997**, *13*, 80.
9. Cheng, T. R.; Huang, C. H.; Gan, L. B. *J. Mater. Chem.* **1997**, *7*, 631.
10. Wu, D. G.; Huang, C. H.; Gan, L. B.; Zhang, W.; Zheng, J.; Luo, H. X.; Li, N. Q. *J. Phys. Chem. B* **1999**, *103*, 4377.
11. Li, F. Y.; Zheng, J.; Huang, C. H.; Jin, L. P.; Zhuang, J. Y.; Guo, J. Q.; Zhao, X. S.; Liu, T. T. *J. Phys. Chem. B* **2000**, *104*, 5090.

12. Lang, A. D.; Zhai, J.; Huang, C. H.; Gan, L. B.; Zhao, Y. L.; Zhou, D. J.; Chen, Z. D. *J. Phys. Chem. B* **1998**, *102*, 1424.
13. Zhai, J.; Huang, C. H.; Wei, T. X.; Gan, L. B.; Cao, H. *Polyhedron* **1999**, *18*, 1513.
14. Wu, D. G.; Huang, C. H.; Huang, Y. Y.; Gan, L. B.; Yu, A. Q.; Ying, L. M.; Zhao, X. S. *J. Phys. Chem. B* **1999**, *103*, 7130.
15. Zhai, J.; Wei, T. X.; Huang, C. H. *Thin Solid Films* **2000**, *370*, 248.
16. Wang, Z. S.; Li, F. Y.; Huang, C. H.; Wang, L.; Wei, M.; Jin, L. P.; Li, N. Q. *J. Phys. Chem. B* **2000**, *104*, 9676.
17. Li, F. Y.; Zheng, J.; Huang, C. H.; Jin, L. P.; Huang, Y. Y.; Guo, J. Q.; Liu, T. T.; Zhao, X. S. *Appl. Surf. Sci.* **2000**, *161*, 178.
18. Huang, Y. Y.; Cheng, T. R.; Li, F. Y.; Huang, C. H.; Wang, S. F.; Huang, W. T.; Gong, Q. H. *J. Phys. Chem. B* **2002**, *106*, 10041.
19. Qin, C. X.; Wang, J. J.; Li, Y.; Xie, H. D.; Wang, X. B.; Dai, L. X.; Wang, X. M.; Chen, G. Q. *J. Appl. Polym. Sci.* **2009**, *113*, 1448.
20. Kabatc, J.; Paczkowski, J. *J. Appl. Polym. Sci.* **2010**, *117*, 2669.
21. Wang, L. Y.; Gao, L. H.; Wang, K. Z. *Acta Chim. Sinica* **2003**, *61*, 1877.
22. Gao, L. H.; Jiang, W. C.; Wang, K. Z. *J. Nanosci. Nanotechnol.* **2011**, *11*, 9813.
23. Gao, L. H.; Wang, K. Z.; Wang, L. Y. *J. Nanosci. Nanotechnol.* **2011**, *11*, 9861.
24. Gao, L. H.; Wang, K. Z.; Wang, L. Y. *J. Nanosci. Nanotechnol.* **2010**, *10*, 2108.
25. Gao, L. H.; Hu, X. J.; Zhang, D. S.; Guo, Y.; Wang, K. Z. *J. Nanosci. Nanotechnol.* **2008**, *8*, 1355.
26. Gao, L. H.; Wang, L. Y.; Wang, K. Z. *Solid State Phenomena* **2007**, *121–123*, 457.
27. Zhang, Y. Q.; Gao, L. H.; Wang, K. Z.; Song, Y. L.; Jiang, L.; Zhu, D. B. *Solid State Phenomena* **2007**, *121–123*, 449.
28. Yu, J. H.; Li, F. Y.; Wang, X. S.; Huang, Y. Y.; Zhang, B. W.; Huang, C. H.; Cao, Y. *Opt. Mater.* **2002**, *21*, 467.
29. Gao, L. H.; Sun, Q. L.; Wang, K. Z. *J. Colloid Interface Sci.* **2013**, *393*, 92.
30. Chen, X.; Gao, L. H.; Zheng, Z. B.; Wang, K. Z. *Mater. Res. Bull.* **2013**, *48*, 595.
31. Gao, L. H.; Sun, Q. L.; Qi, J. M.; Lin, X. Y.; Wang, K. Z. *Electrochim. Acta* **2013**, *92*, 236.
32. Gao, L. H.; Sun, Q. L.; Lin, X. Y.; Qi, J. M.; Wang, K. Z. *Colloids Surf. A* **2013**, *423*, 162.
33. Gao, L. H.; Lu, S.; Su, J. P.; Wang, K. Z. *J. Nanosci. Nanotechnol.* **2013**, *13*, 1377.
34. Tjipto, E.; Quinn, J. F.; Caruso, F. *Langmuir* **2005**, *21*, 8785.
35. Jelly, E. E. *Nature* **1936**, *138*, 1009.
36. Wang, Z. S.; Huang, Y. Y.; Huang, C. H.; Zheng, J.; Cheng, H. M.; Tian, S. *J. Synth. Met.* **2000**, *114*, 201.
37. Gao, L. H.; Wang, K. Z.; Cai, L.; Zhang, H. X.; Jin, L. P.; Huang, C. H.; Gao, H. J. *J. Phys. Chem. B* **2006**, *110*, 7402.
38. Chen, W.; Nikiforov, M. P.; Darling, S. B. *Energy Environ. Sci.* **2012**, *5*, 8045.
39. Polymeropoulos, E. E.; Möbius, D.; Kuhn, H. *Thin Solid Films* **1980**, *68*, 173.
40. Wei, T. X.; Zhai, J.; Ge, J. H.; Gan, L. B.; Huang, C. H.; Luo, G. B.; Ying, L. M.; Liu, T. T.; Zhao, X. S. *Appl. Surf. Sci.* **1999**, *151*, 153.
41. Gaines, G. L., Jr. *Angew. Chem. Int. Ed.* **1987**, *26*, 341.
42. Sereno, L.; Silbeer, J. J.; Otero, L.; Bohorquez, M. D. V.; Moore, A. L.; Moore, T. A.; Gust, D. *J. Phys. Chem.* **1996**, *100*, 814.
43. Kim, Y. S.; Liang, K.; Law, K. Y.; Whitten, D. G. *J. Phys. Chem.* **1994**, *98*, 984.
44. Wang, K. Z.; Gao, L. H.; Bai, G. Y.; Jin, L. P. *Inorg. Chem.* **2002**, *41*, 3353.
45. Imahori, H.; Norieda, H.; Nishimura, Y.; Yamazaki, I.; Higuchi, K. *J. Phys. Chem. B* **2000**, *104*, 1253.
46. Grätzel, M. *J. Photoch. Photobiol. C* **2003**, *4*, 145.
47. Fan, S. H.; Zhang, A. G.; Ju, C. C.; Gao, L. H.; Wang, K. Z. *Inorg. Chem.* **2010**, *49*, 3752.
48. Fan, S. H.; Wang, K. Z.; Yang, W. C. *Eur. J. Inorg. Chem.* **2009**, *4*, 508.
49. Fan, S. H.; Zhang, A. G.; Ju, C. C.; Wang, K. Z. *Solar Energy* **2011**, *85*, 2497.